Springer

KSME

Journal of Mechanical Science and Technology 33 (8) (2019) 3943~3953
www.springerlink.com/content/1738-494x(Print)/1976-3824(Online)
DOI 10.1007/s12206-019-0739-6

Mesh stiffness analysis of beveloid gears for the rotating vector transmission †

Yucheng Huang, Xuesong Du*, Caichao Zhu, Gaoxiang Ni, Najeeb Ullah and Hao Liu

The State Key Laboratory of Mechanical Transmissions, Chongqing University, Chongqing, China

(Manuscript Received February 9, 2019; Revised April 23, 2019; Accepted May 7, 2019)

Abstract

This paper investigates the meshing stiffness of beveloid gears in the beveloid rotate vector (BRV) transmission. It is a new kind of transmission evolved from rotate vector (RV) reducer. In the BRV transmission, the beveloid gear is a kind of involute gear with a bevel angle. The BRV transmission have high power density, large transmission ratio and high precision in geared coupled systems. However, there is rare systematic research conducted on the meshing stiffness analysis of the BRV transmission at present. Based on the loaded contact finite element analysis principle, a meshing stiffness analysis model for beveloid gears is established. The influence of different factors such as pitch cone angle, addendum coefficient, load and rim structure parameters of external gear on meshing stiffness are studied. The results show that the pitch cone angle and addendum coefficient have little effect on the shape of the meshing stiffness curve, but they have a significant influence on the amplitude of meshing stiffness. In contrast, the load can affect both the shape and the amplitude of the meshing stiffness curve obviously. Also, the size of scallop-hole and rim thickness have a great impact on the amplitude of the meshing stiffness. The prescribed piece of study can provide a better understanding for gear researchers in order to understand the influence of different parameters on dynamic characteristics analysis of the BRV transmission systems.

Keywords: RV transmission; Few tooth difference drive; Beveloid gears; Meshing stiffness; FEM

1. Introduction

The beveloid rotate vector (BRV) Reducer is a high-performance precision mechanical transmission device, which has the advantages of large transmission ratio, high power density, high torsional rigidity, high transmission precision, strong impact resistance and long service life. Therefore, BRV reducers can be widely used in precision instruments, aerospace, industrial robots and other fields. As the important components, the beveloid gears can seriously affect the performance of the BRV Reducer. So it is very significant to analyze the meshing stiffness of the beveloid gears.

Mettitt [1] firstly proposed Beveloid gears with anti-backlash, eliminating installation errors and ease of processing, etc., which makes it one of the most important gearing parts. Subsequently, Mitome [2] proposed a tilting working-axis taper hobbing method and a table sliding roller method to solve the manufacturing problem of the beveloid gears. Liu et al. [3] investigated the influence of work holding equipment errors on mesh behavior and gear flank geometry of face-hobbed hypoid gear based on accurate mesh model which established from generated process.

Stiffness is one of the main excitations of meshing vibration in gear system, and obtaining the meshing stiffness of gears has always been the most important task in the study of gear system dynamics. Cornell [4] simplified the involute spur gear teeth into trapezoidal cantilever beams in order to calculate their single tooth meshing stiffness with material mechanics and tooth surface meshing stress. In addition, Huang and Liu [5] simplified the spur gears into variable-section Timoshenko beams, and described the gear blanks and tooth surfaces with polynomials so that the dynamic meshing stiffness of the spur gears can be calculated. Conry and Seireg [6, 7] proposed a mathematical model to calculate the load distribution of helical gears, and calculated the meshing stiffness of helical gears. Based on the slicing method, an improved analytical method (IAM) was proposed by Feng et al. [8-10] to calculate the time-varying mesh stiffness (TVMS) of the helical gear pair. Additionally, the effects of helix angle, tooth width, correction coefficient and friction coefficient on time-varying mesh stiffness was studied. Han et al. [11] is the first one who proposed a calculation method for the meshing stiffness of helical gears, considering friction and analyzed the influence of friction on the total meshing stiffness. Wan et al. [12] studied the influence of helix angle and normal modulus on the meshing stiffness, and concluded that, with the increase of the helix angle or the width of the surface, the meshing stiffness fluctuates less and the impact of the normal modulus shows the opposite trend. Later on, some scholars have used finite element method to study the gear mesh stiffness.

*Corresponding author. Tel.: +86 13638360236, Fax.: +86 23 65111192
E-mail address: duxs@cqu.edu.cn
† Recommended by Associate Editor Ki-Hoon Shin

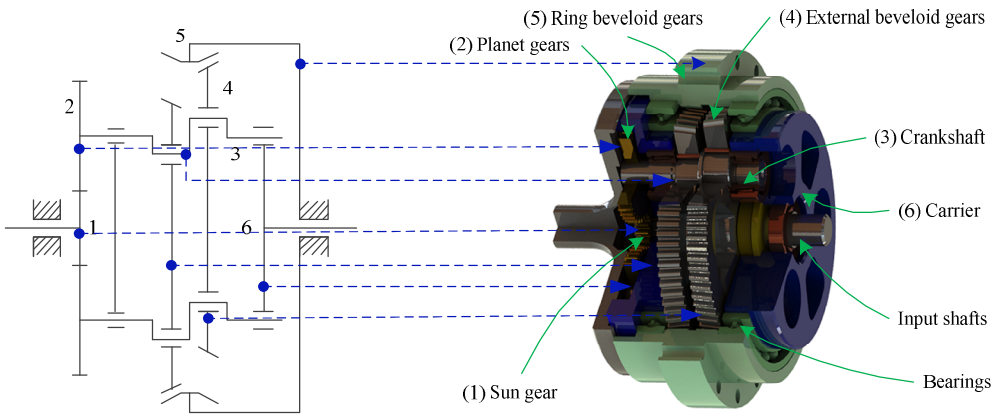

Fig. 1. Schematic diagram of the BRV transmission and 3D structure.

Sirichai [13] established a general nonlinear finite element analysis model for static meshing gears pair, which is used to derive the torsional meshing stiffness of involute cylindrical gears. Then, Wang [14] further refined his work. Lin et al. [15-17] established a finite element model by considering the nonlinearity of the contact deformation. Using this model, the gear meshing stiffness for static load during interaction was obtained. Chaari et al. [18] analyzed the meshing stiffness of a gear pair and compared with the analysis results of the finite element model. Based on the tooth surface contact method, Li [19] studied the loaded tooth contact analysis to investigate the influence of the addendum on the meshing stiffness. Zhan et al. [20] proposed a meshing stiffness determination method by using NX, ANSYS Workbench and quasi-static algorithm (QSA) in order to analyze the influence of tooth tip radius and gear pair misalignment on time-varying mesh stiffness. Furthermore, the influence of the flexible bearing support on the meshing stiffness for the beveloid gears is also studied. Liang et al. [21] established a finite element analysis model to study the gear meshing stiffness of flexible bearing support. It was found that fatigue load caused the expansion of gear tooth crack, which further led to the reduction of gear meshing stiffness.

In short, a lot of scholars conducted their research on analysis and calculation method of meshing stiffness for parallel-shaft straight and parallel-shaft helical gear transmission systems, but the systematic study on the analysis of meshing stiffness for parallel-shaft beveloid gears in the BRV transmission is rare. Therefore, this paper takes the beveloid gears in the BRV transmission as the research object. In accordance with the finite element method, the impact of different factors such as the pitch cone angle, the addendum coefficient, the load and the geometry of the gear rim on meshing stiffness for beveloid gears transmission are studied.

2. Transmission principle of BRV transmission and tooth-surface equation of beveloid gears

2.1 Transmission principle of BRV transmission

The transmission principle of the BRV transmission system is shown in Fig. 1 which consists of an involute planetary gear and a beveloid planetary gear of few tooth difference.

The technical organization of the proposed system is as follows: the sun gear on the input shaft and the planetary gear are represented by 1 and 2. The crankshaft and the external beveloid gears are represented by 3 and 4, while 5 and 6 stand for the ring beveloid gear and the carrier (the output component), respectively. When the sun gear 1 is driven by the motor to rotate clockwise, the planetary gear 2 rotates counterclockwise and revolve around the sun gear 1. In addition, the planetary gear 2 drives the beveloid gears 4 to revolve by the crankshaft 3. When the ring beveloid gear 5 is fixed, the carrier 6 rotates clockwise by giving rise to output power, and the transmission ratio can be described as shown in Eq. (1).

$$i = 1 + \frac{z_2}{z_1} \cdot \frac{z_5}{(z_5 - z_4)} \tag{1}$$

where z_1 is the tooth number of the sun gear, z_2 is the tooth number of the planetary gear, z_4 is the tooth number of beveloid gears and z_5 is the tooth number of the ring beveloid gear.

In order to get a large transmission ratio, it usually takes $z_5 - z_4 = 1 \sim 2$ to make the beveloid gear 4 and the ring beveloid gear 5 to be a beveloid transmission with few tooth difference.

2.2 Tooth-surface equation of beveloid gears

According to the generation theory proposed by Merritt [1], the tooth surface of the beveloid gears can be regarded as being formed by the tooth of the shaper cutter. In order to obtain the tooth surface equation of the beveloid gears, the coordinate system is established.

As shown in Fig. 2, three typical positions for the shaper cutter are defined as the upper layer, the middle layer and the lower layer. On the middle layer, the pitch circles of the shaper cutter and the beveloid gears blank are tangent to each other with the modification coefficient as zero. On upper layer,

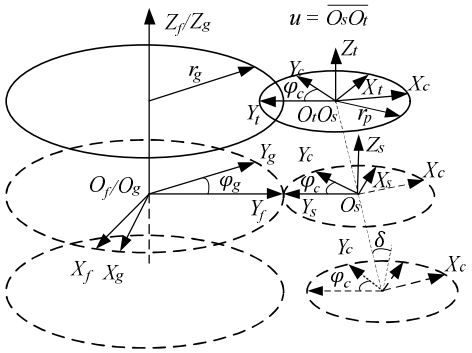

(a) External beveloid gear

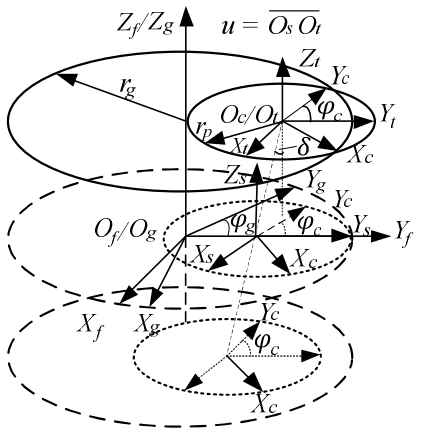

(b) Ring beveloid gear

Fig. 2. Beveloid gears machining coordinate system.

the modification coefficient is negative for external beveloid gear (which is positive for ring beveloid gear). On lower layer, the modification coefficient is positive for external beveloid gear (which is negative for ring beveloid gear). Coordinate $S_s\left(x_s,y_s,z_s\right)$ is fixed to the frame while coordinate $S_t\left(x_t,y_t,z_t\right)$ is fixed to the pitch circle center of the shaper cutter with only the translational direction along the cutting direction. $S_c\left(x_c,y_c,z_c\right)$ is fixed to the shaper cutter and represents the shaper cutter normal section. $S_f\left(x_f,y_f,z_f\right)$ and $S_g\left(x_g,y_g,z_g\right)$ are fixed to the frame and beveloid gears blank, respectively [22].

The tooth surface equation [22] of the beveloid gears is derived by the relative motion relationship between the mathematical equations of the shaper cutter normal section and the blank, which is expressed in the coordinate system $S_g\left(x_g,y_g,z_g\right)$ as follows.

Where δ and φ_g are the pitch cone angle and the corresponding rotation angle of the beveloid gears, respectively. Whereas, φ_c is the rotation angle of shaper cutter, r_p is the pitch circle radius of the shaper cutter. In addition, r_g is the pitch circle radius of beveloid gears and u is the translational displacement of the shaper cutter. The tooth surface of the ring beveloid gear and external beveloid gear are established by the Eqs. (2) and (3).

The tooth surface equation of the beveloid gears.

$$\begin{bmatrix} X_g \\ Y_g \\ Z_g \end{bmatrix} = \begin{bmatrix} X_c\cos\left(\varphi_c-\varphi_g\right)+Y_c\cos\left(\varphi_c-\varphi_g\right)-\left(u\sin\delta+r_g+r_p\right)\sin\varphi_g \\ -X_c\cos\left(\varphi_c-\varphi_g\right)+Y_c\cos\left(\varphi_c-\varphi_g\right)+\left(u\sin\delta+r_g+r_p\right)\cos\varphi_g \\ u\cos\delta \end{bmatrix}. \quad (2)$$

The tooth surface equation of the ring beveloid gear.

$$\begin{bmatrix} X_g \\ Y_g \\ Z_g \end{bmatrix} = \begin{bmatrix} X_c\cos\left(\varphi_c-\varphi_g\right)-Y_c\cos\left(\varphi_c-\varphi_g\right)+\left(u\sin\delta+r_g-r_p\right)\sin\varphi_g \\ X_c\cos\left(\varphi_c-\varphi_g\right)+Y_c\cos\left(\varphi_c-\varphi_g\right)+\left(u\sin\delta+r_g-r_p\right)\cos\varphi_g \\ u\cos\delta \end{bmatrix}. \quad (3)$$

3. Finite element analysis model of beveloid gears

It is justifiable by the Eq. (6) that the meshing stiffness calculation of the BRV transmission system requires the tooth contact force on the tooth surface and the combined elastic deformation. To considering the influence of rim structure of external gear on the meshing stiffness, the meshing analysis is carried out by the finite element method with CAE software ABAQUS. And the tooth contact force and combined elastic deformation are extracted by output databases in ABAQUS.

The basic parameters of the prototype used in this paper are shown in Table 1, and the finite element analysis model is established as follows.

(1) According to Eqs. (2) and (3), point-sets on the tooth surface of the outer and ring beveloid gear tooth are calculated, respectively. The tooth surface of ring beveloid gear and external beveloid gear are constructed in the 3D modeling software (Pro/E). The parameters of the hub part are designed according to the drawings in order to establish ring beveloid gear and external beveloid gear as shown in Fig. 3, which are assembled based on the design dimensions. Due to the different rim thickness, the area where the gear teeth are located is divided into the rigid zone and the flexible zone, and the pairs of teeth are numbered as 1~20 for the external beveloid gear (which is 1'~20' for the ring beveloid gear) as presented in Fig. 4.

(2) The contact type of gear tooth pairs is frictionless, and its tooth surface is discretized. Moreover, hexahedron is selected as the grid unit type, and the FE model of external and ring beveloid gear has 429142 and 256843 elements, respectively.

(3) In the setting of the boundary condition, the ring beveloid gear is completely restrained, and the external beveloid gear can be rotated along its own axis and revolved along the axis of ring beveloid gear, so that the external beveloid gear can make a composite movement in a plane perpendicular to its axis. An angular displacement θ = 4.6 degree is applied in the rotational direction of the external beveloid gear to ensure that at least one teeth has completely meshed. The rated torque T = 206 Nm is applied on the three bearing holes in the direction of rotation along the external beveloid gear's axis, and the direction is the same with the angular displacement as shown in Fig. 5.

Table 1. Gear parameters of the BRV transmission.

The first stage gear parameter		Sun gear	Planetary gear
Tooth number	z	18	36
Module/mm	m_t	1.25	1.25
Pressure angle/deg	α	20	20
Modification coefficient	x	0.2	-0.2
Face width/mm	b	11	10
Coefficient of tip clearance	c	0.25	0.25
Addendum coefficient	h_a	1	1
Modulus of elasticity/GPa	E	209	209
Poisson's ratio	v	0.295	0.295
The second stage gear parameter		External beveloid gear	Ring beveloid gear
Tooth number	z	78	80
Module/mm	m_t	1.5	1.5
Pressure angle/deg	α	20	20
Modification coefficient	x	0.7~1	1.123~1.423
Pitch cone angle/deg	δ	2.5	2.5
Face width/mm	b	10	10
Coefficient of tip clearance	c	0.25	0.25
Addendum coefficient	h_a	0.7	0.7
Modulus of elasticity/GPa	E	209	209
Poisson's ratio	v	0.295	0.295

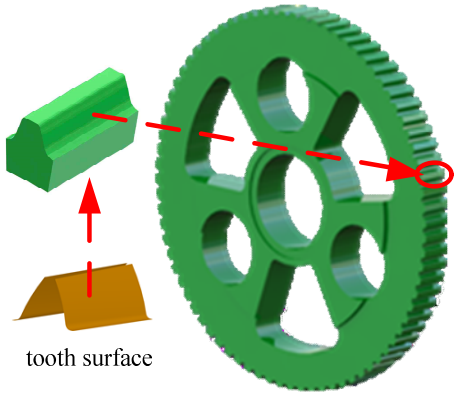

(a) External beveloid gear

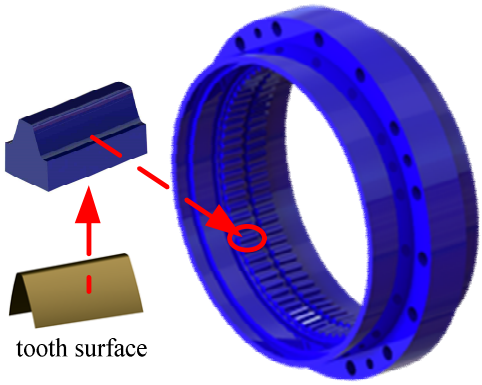

(b) Ring beveloid gear

Fig. 3. The 3D model of the beveloid gears.

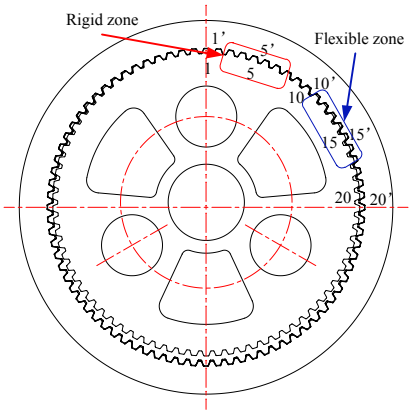

Fig. 4. Gear number of the beveloid gears.

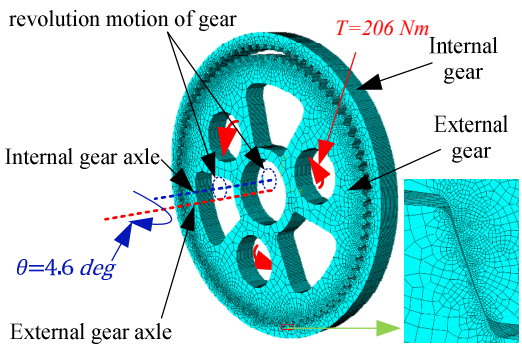

Fig. 5. Finite element model the beveloid gears.

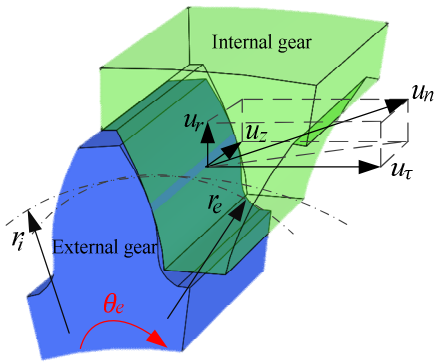

Fig. 6. Combined elastic deformation of beveloid gear pair.

4. Results and discussion

4.1 Formula of meshing stiffness

The calculation formula of single tooth meshing stiffness (Chaari et al., 2009) is shown in Eq. (4).

$$k_n = \frac{F_n}{u_n} \tag{4}$$

where F_n is normal contact force, u_n is combined elastic deformation of a single pair of teeth.

The numerical solution of the meshing stiffness is obtained by finite element method generally. The combined elastic deformation of the tooth includes the relative displacement along axial-direction u_z, the relative radial displacement u_r and the relative tangential displacemen u_τ, which is shown in Fig. 6. So the combined elastic deformation are calculated as shown in Eq. (5).

$$u_n = \sqrt{u_z^2 + u_r^2 + u_\tau^2}. \tag{5}$$

The number of meshing teeth for the beveloid gears pair is relatively larger compared with spur gear. When combined contact occurs, the calculation formula of the combined meshing stiffness of the gear can be calculated as following.

$$k_m = \sum_{i=1}^{p} k_{ni} \tag{6}$$

where p is the number of teeth for those which are in contact at the same time.

4.2 Meshing stress and deformation of the beveloid gears

For studying the variation law of the contact force for the beveloid gears pair, the contact force of each pair of meshing teeth is extracted in one meshing period as shown in Fig. 7. It can be seen that the contact force changes periodically with the change of the meshing tooth number, and the contact force of each tooth has a parabolic nonlinear change as shown in Fig. 7(a).

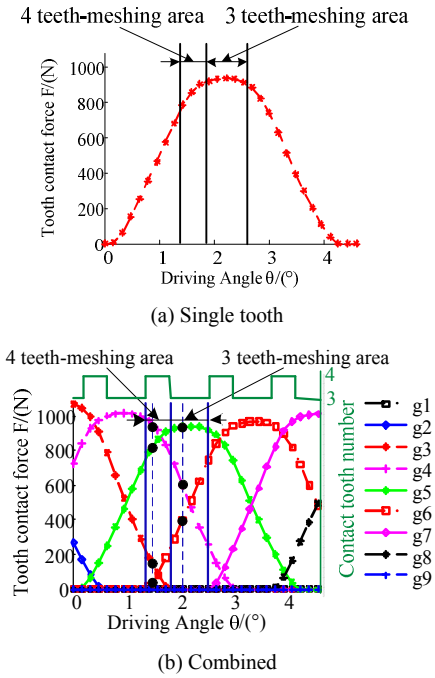

(a) Single tooth

(b) Combined

Fig. 7. Tooth contact force and contact tooth number.

The maximum contact force of the tooth pair in the 3-tooth meshing zone is 921.3 N. The maximum contact force of the tooth pair in the 4-tooth meshing zone was only reduced by 3.6 %. which is 887.5 N. The load distribution of the tooth is not uniform after being loaded, so the maximum contact force cannot be linearly reduced as the number of meshing teeth increasing linearly.

The elastic deformation of each node on the tooth surface is different. In the calculation of the combined elastic deformation of the tooth, the method is performed as follows: firstly, the elastic deformation of each node on the surface of the tooth surface is extracted as shown in Fig. 8(a). Then, the mean of the deformation amount of each node is obtained correspondingly, thereby obtaining the total elastic deformation amount of the meshing tooth pair as shown in Fig. 8(b).

4.3 Impact of flexible zone and rigid zone on meshing stiffness

The contact force and combined elastic deformation of each tooth pair have been calculated in Sec. 5.1, then, the single tooth meshing stiffness and the combined meshing stiffness can be calculated by Eqs. (2)-(4). In order to study the influence of the rigid zone and the flexible zone on the single tooth meshing stiffness and combined meshing stiffness, the data of the No. 5 gear tooth in the rigid zone and the No. 15 gear tooth in the flexible zone were extracted.

The single tooth meshing stiffness and combined meshing stiffness are shown in Figs. 9 and 10, respectively. It can be seen that in a meshing period, the single tooth meshing stiffness curves of the flexible zone and the rigid zone are similar,

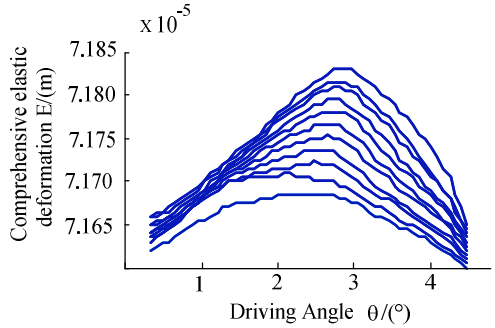

(a) Elastic deformation of the nodes

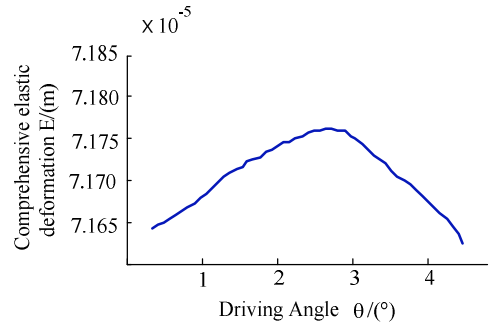

(b) Combined elastic deformation

Fig. 8. Combined elastic deformation of contact tooth pair.

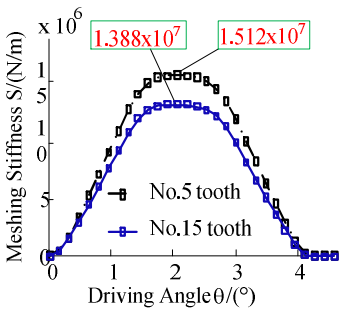

Fig. 9. Single tooth meshing stiffness.

which are approximate parabola, but the single tooth meshing stiffness peak of the flexible zone is reduced by about 10.0 % compared with the rigid zone. The average value of the combined combined meshing stiffness of the flexible zone reduces by about 9.1 % compared with the rigid zone, so the rim thickness has a significant influence on the stiffness of the gear. The peaks and valleys of the combined meshing stiffness for the flexible zone and the rigid zone correspond to the 3-tooth meshing zones and 4-tooth meshing zones respectively, but the fluctuation amplitude is not obvious.

4.4 Impact of basic parameters on meshing stiffness

Among the basic parameters, the pitch cone angle and the addendum coefficient can well reflect the geometrical characteristics of the beveloid gears. Therefore, the influence of these two parameters on the meshing stiffness is studied.

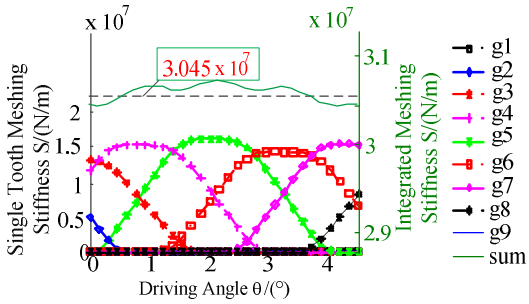

(a) No. 5 tooth

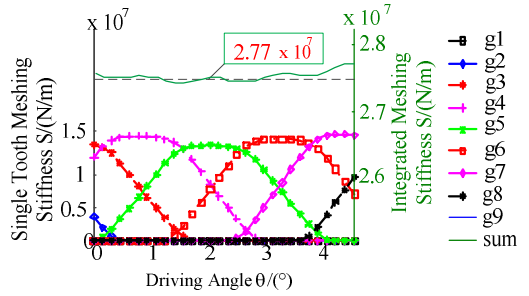

(b) No. 15 tooth

Fig. 10. Combined meshing stiffness.

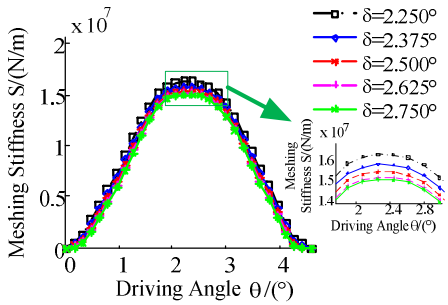

(a) No. 5 tooth

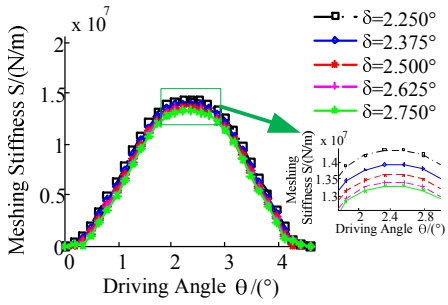

(b) No. 15 tooth

Fig. 11. Single tooth meshing stiffness.

4.4.1 Effect of pitch cone angle on meshing stiffness

The rest of the factors were kept unchanged as follows: The addendum coefficient $h_a = 0.7$, the load $T = 206$ Nm, the waist angle $\varnothing = 50°$ and the rim coefficient $m_B = 3$. According to the finite element model mentioned above, pitch cone angle δ of the gear pair is selected as follows: 2.25°,

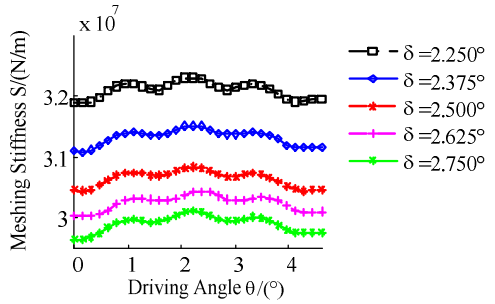

(a) No. 5 tooth

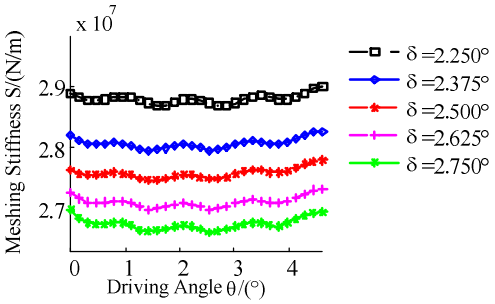

(b) No. 15 tooth

Fig. 12. Combined meshing stiffness.

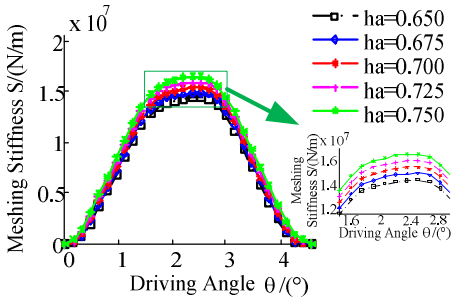

(a) No. 5 tooth

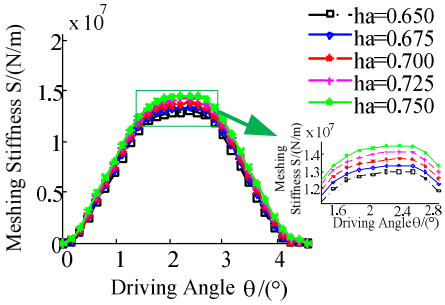

(b) No. 15 tooth

Fig. 13. Single tooth meshing stiffness.

2.375°, 2.5°, 2.625° and 2.75° to calculate the single tooth mesh stiffness as shown in Fig. 11 and combined meshing stiffness as shown in Fig. 12.

It can be seen that the variation of pitch cone angle does not affect the single tooth mesh stiffness, the combined combined meshing stiffness of the flexible zone and the rigid zone during one meshing period. When the pitch cone angle increases from 2.25° to 2.75°, the single-tooth meshing stiffness of the No. 5 tooth and the No. 15 tooth nonlinearity decreases by 7.4 % and 7.8 %, respectively. While, the combined combined meshing stiffness nonlinearity decreases by 6.8 % and 7.3 %, respectively.

4.4.2 Effect of addendum coefficient on meshing stiffness

The rest of the factors were kept unchanged as follows: The pitch cone angle $\delta = 2.5°$, the load $T = 206$ Nm, the waist angle $\varnothing = 50°$ and the rim coefficient $m_B = 3$. According to the above finite element model, addendum coefficient h_a is selected as follows: 0.65, 0.675, 0.7, 0.725 and 0.75 in order to calculate the single tooth mesh stiffness as shown in Fig. 13. Whereas, combined meshing stiffness is shown in Fig. 14.

It can be seen that as the addendum coefficient increases, the full height of the tooth and contact ratio increase, so that the single tooth meshing stiffness and the combined meshing stiffness increase in one meshing period. When the addendum coefficient h_a increases from 0.65 to 0.75°, the single-tooth meshing stiffness of the No. 5 tooth and the No. 15 tooth linearly increases by 10.9 % and 12.3 % respectively, and the combined combined meshing stiffness linearly increases by 11.9 % and 14.7 %, respectively.

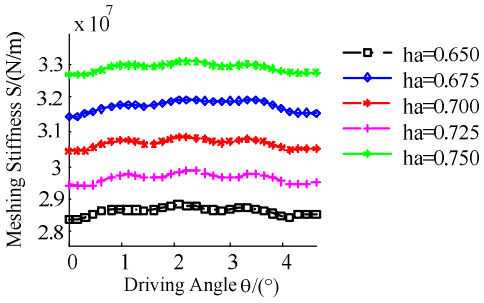

(a) No. 5 tooth

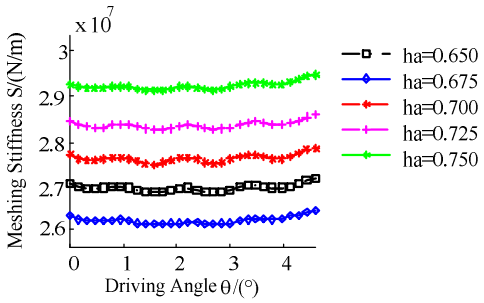

(b) No. 15 tooth

Fig. 14. Combined meshing stiffness.

4.5 Effect of load on meshing stiffness

The rest of the factors were kept unchanged as follows: the pitch cone angle $\delta = 2.5°$, the addendum coefficient $h_a = 0.7$, the waist angle $\varnothing = 50°$ and the rim coefficient $m_B = 3$. In order to study the effect of load on the meshing stiffness, the load T is selected as follows: 50 Nm, 100 Nm,

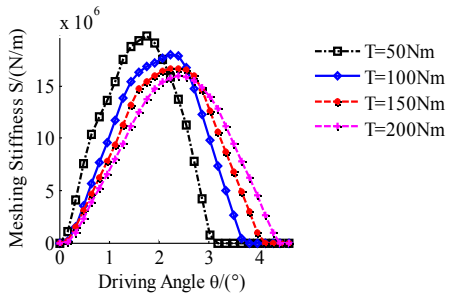

(a) No. 5 tooth

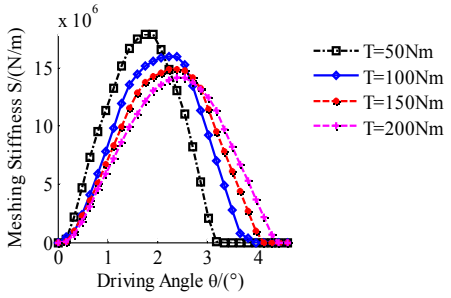

(b) No. 15 tooth

Fig. 15. Single tooth meshing stiffness.

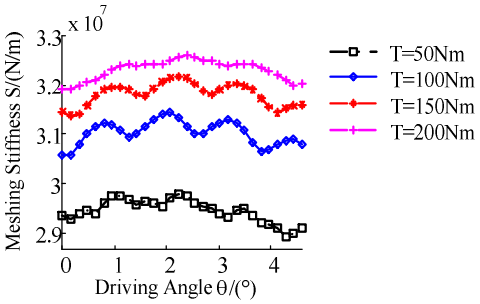

(a) No. 5 tooth

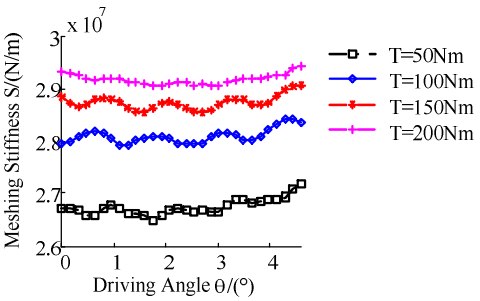

(b) No. 15 tooth

Fig. 16. Combined meshing stiffness.

150 Nm, and 200 Nm to calculate the single tooth mesh stiffness as shown in Fig. 15 and combined meshing stiffness is shown in Fig. 16.

It can be seen that as the load increases, the number of pairs of tooth involved in meshing increases with the variation in load distribution as shown in Fig. 7(b). This further leads to the single tooth meshing stiffness of the flexible zone or the

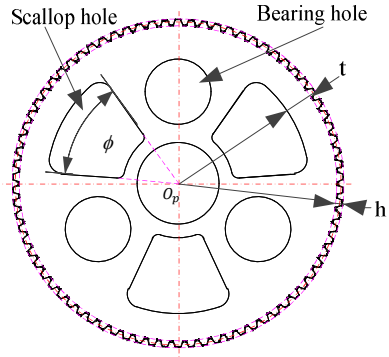

Fig. 17. Geometric structure of external beveloid gear.

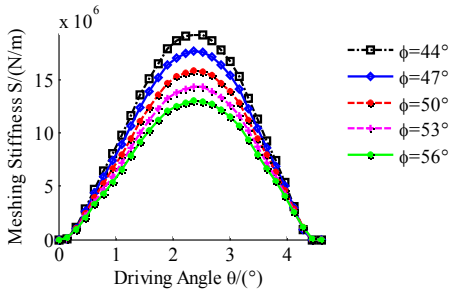

(a) No. 5 tooth

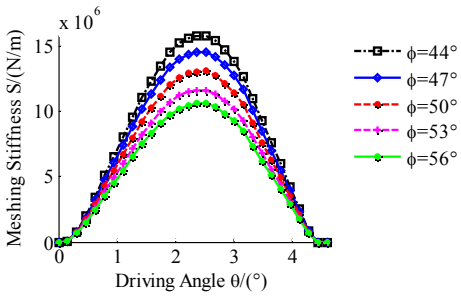

(b) No. 15 tooth

Fig. 18. Single tooth meshing stiffness.

rigid zone nonlinearity which also decreases as the total meshing stiffness increases in a nonlinear way. At the same time, it can be found that with the increase in load, the fluctuation of the combined meshing stiffness goes downward.

4.6 Effect of rim structure parameters on meshing stiffness

In the BRV transmission, since the crankshaft bearing needs to be mounted on the external beveloid gear at the bearing hole, and the carrier needs to pass through the scallop-hole, so the bearing hole and the scallop-hole are designed on the external beveloid gear, which result in differences in rim thickness, as shown in Fig. 17. In the figure, t is rim thickness, h is full height of the tooth and $\varnothing$ is waist angle.

4.6.1 Effect of waist angle on meshing stiffness

The rest of the factors were kept unchanged as follows: The

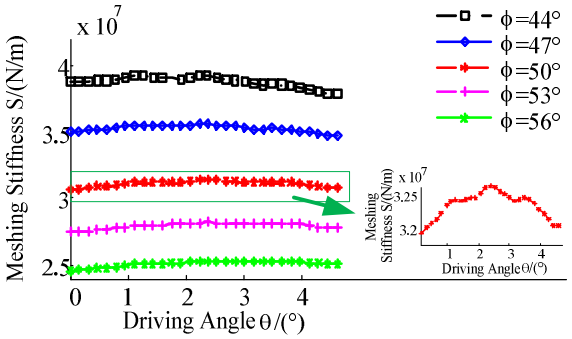

(a) No. 5 tooth

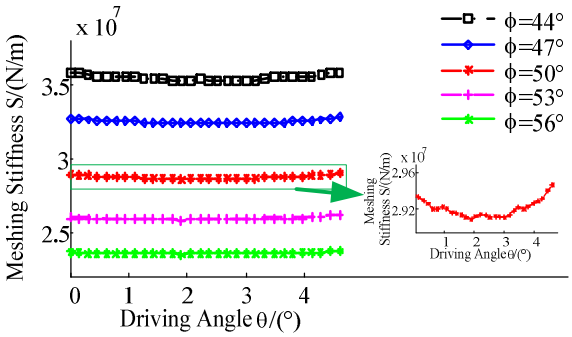

(b) No. 15 tooth

Fig. 19. Combined meshing stiffness.

pitch cone angle $\delta = 2.5°$, the addendum coefficient $h_a = 0.7$, the load T = 206 Nm and the rim coefficient $m_B = 3$. Waist angle $\varnothing$ is selected as follows: 44°, 47°, 50°, 53° and 56° to obtain the single tooth mesh stiffness as shown in Fig. 18 and combined meshing stiffness as shown in Fig. 19.

It can be seen that the single tooth mesh stiffness and the combined combined meshing stiffness of the flexible zone and the rigid zone gradually reduced as the waist angle increases during one meshing period. When the waist angle increases from 44° to 56°, the single-tooth meshing stiffness of the No. 5 tooth and the No. 15 tooth nonlinearity decreases by 38.2 % and 43.8 % respectively, and the combined meshing stiffness nonlinearity decreases by 48.6 % and 50.6 %, respectively.

4.6.2 Effect of rim coefficient on meshing stiffness

Rim coefficient m_B,

$$m_B = \frac{t}{h}. \tag{7}$$

The rest of the factors were kept unchanged as follows: the pitch cone angle $\delta = 2.5°$, the addendum coefficient $h_a = 0.7$, the load T = 206 Nm and the waist angle $\varnothing = 50°$. According to the finite element model mentioned above, rim coefficient m_B is selected as follows: 3, 5, 7 and 9 to get the single tooth mesh stiffness as shown in Fig. 20 and combined meshing stiffness as shown in Fig. 21.

It can be seen that as the rim coefficient increases, the rim

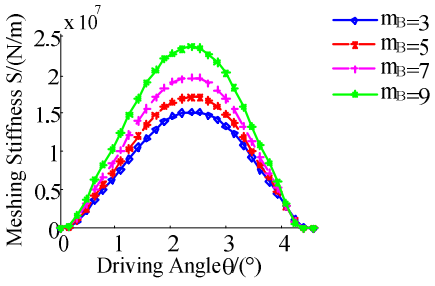

(a) No. 5 tooth

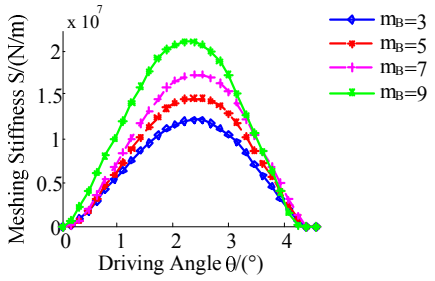

(b) No. 15 tooth

Fig. 20. Single tooth meshing stiffness.

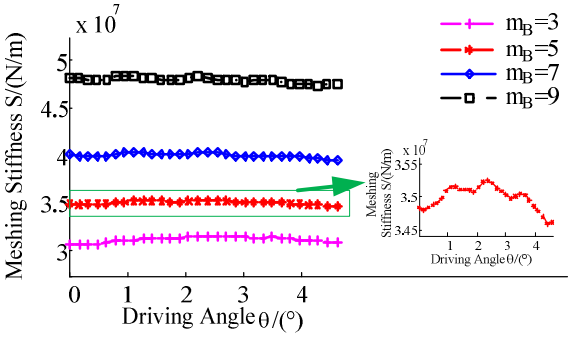

(a) No. 5 tooth

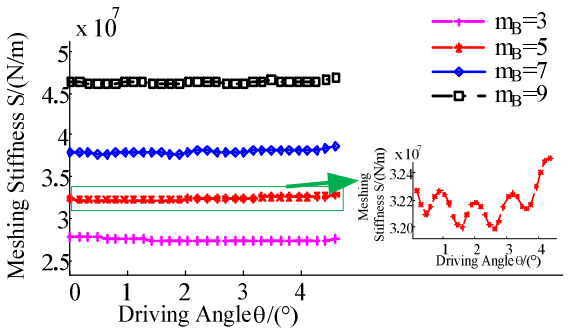

(b) No. 15 tooth

Fig. 21. Combined meshing stiffness.

thickness of the flexible zone becomes larger which causes the single tooth mesh stiffness and the combined combined meshing stiffness of the flexible zone and the rigid zone to gradually increase in one meshing period. When the rim coefficient increases from 3 to 9, the single-tooth meshing stiffness of the

No. 5 tooth and the No. 15 tooth decreases by 35.6 % and 41.2 %, respectively, while the combined combined meshing stiffness decreases by 35.8 % and 39.7 %, respectively. This means, rim coefficient has an inverse relation with single as well as combined meshing stiffness of the system.

5. Conclusion

(1) The 3D models of the BRV gear transmission system were derived. Then, the finite element models of the beveloid gears in the BRV gear transmission system were proposed, by considering the influence of different factors, such as pitch cone angle, addendum coefficient, load and rim structure of external beveloid gear. In addition, the resulting of meshing stiffness influenced by the various factors is investigated.

(2) The pitch cone angle and the addendum coefficient have little effect on the curve shape of the meshing stiffness, yet have a big influence on the amplitude. In addition, the meshing stiffness increase significantly as the rim coefficient rise, while reduce drastically when the waist angle goes up.

(3) The research shows that the meshing stiffness on the flexible zone is about 10.0 % lower than that of the rigid zone. Moreover, the load highly affects the variation law of the meshing stiffness and the amplitude.

Acknowledgements

The authors would like to thank the National Natural Science Foundation of China (Grant No. 51575060) and Key Research and Development Project of Chongqing Science and Technology Commission (Grant No. cstc2017rgzn-zdyfX0038).

References

[1] H. E. Merritt, *Gears*, 3rd edition, Isaac Pitman & Sons (1954).

[2] K. Mitome, Table sliding taper hobbing of conical gear using cylindrical hob, part 1: Theoretical analysis of table sliding taper hobbing, *Journal of Manufacturing Science & Engineering*, 103 (4) (1981) 446-451.

[3] S. Liu, C. Song, C. Zhu, C. Liang and X. Yang, In vestigation on the influence of work holiding equipment errors on contact characteristics of face-hobbed hypoid gear, *Mechanism and Machine Theory*, 138 (2019) 59-111.

[4] R. W. Cornell, Compliance and stress sensitivity of spur gear teeth, *Journal of Mechanical Design,* 103 (2) (1981) 447-459.

[5] K. J. Huang and T. S. Liu, Dynamic analysis of a spur gear by the dynamic stiffness method, *Journal of Sound and Vibration*, 234 (2) (2000) 311-329.

[6] T. F. Conry and A. Seireg, A mathematical programming method for design of elastic bodies in contact, *Journal of Applied Mechanics*, 38 (2) (1971) 387-392.

[7] T. F. Conry and A. Seireg, A mathematical programming technique for the evaluation of load distribution and optimal modifications for gear systems, *Journal of Engineering for Industry,* 11 (1973) 1115-1122.

[8] M. J. Feng and H. Ma, An improved analytical method for calculating time-varying mesh stiffness of helical gears, *Meccanica*, 53 (4-5) (2018) 1131-1145.

[9] R. B. Chen, J. X. Zhou and W. L. Sun, Dynamic characteristics of a planetary gear system based on contact status of the tooth surface, *Journal of Mechanical Science and Technology*, 32 (1) (2018) 69-80.

[10] H. T. Chen, J. K. Fan, S. X. Jing and X. H. Wang, Probabilistic design optimization of wind turbine gear transmission system based on dynamic reliability, *Journal of Mechanical Science and Technology*, 33 (2) (2019) 579-589.

[11] L. Han, L. X. Xu and H. J. Qi, Influences of friction and mesh misalignment on time-varying mesh stiffness of helical gears, *Journal of Mechanical Science and Technology*, 31 (7) (2017) 3121-3130.

[12] Z. G. Wan, H. R. Cao, Y. Y. Zi, W. P. He and Y. M. Chen, Mesh stiffness calculation using an accumulated integral potential energy method and dynamic analysis of helical gears, *Mechanism and Machine Theory*, 92 (2015) 447- 463.

[13] S. Sirichai, Torsional properties of spur gears in mesh using nonlinear finite element analysis, *Ph.D. Thesis*, Curtin University of Technology (1999).

[14] J. D. Wang, Numerical and experimental analysis of spur gears in mesh, *Curtin University of Technology* (2003).

[15] T. Lin, H. Ou and R. Li, A finite element method for 3D static and dynamic contact/impact analysis of gear drives, *Computer Methods in Applied Mechanics and Engineering,* 196 (9-12) (2007) 1716-1728.

[16] T. Kiekbusch, D. Sappok, B. Sauer and I. Howard, Calculation of the combined torsional mesh stiffness of spur gear with two- and three-dimensional parametrical FE models, *Journal Mechanical of Engineering,* 57 (2011) 810-818.

[17] Y. J. Wu, J. J. Wang and Q. K. Han, Contact finite element method for dynamic meshing characteristics analysis of continuous engaged gear drives, *Journal of Mechanical Science and Technology,* 26 (6) (2012) 1671-1685.

[18] F. Chaari, T. Fakhfakh and M. Haddar, Analytical modelling of spur gear tooth crack and influence on gearmesh stiffness, *European Journal of Mechanics, A/Solids,* 28 (3) (2009) 461-468.

[19] S. Li, Effect of addendum on contact strength, bending strength and basic performance parameters of a pair of spur gears, *Mechanism and Machine Theory*, 43 (12) (2008) 1557-1584.

[20] J. Zhan, M. Fard and R. Jazar, A CAD-FEM-QSA integration technique for determining the time-varying meshing stiffness of gear pairs, *Measurement*, 100 (2017) 139-149.

[21] X. Liang, H. Zhang, L. Liu and M. J. Zuo, The influence of tooth pitting on the mesh stiffness of a pair of external spur gears, *Mechanism and Machine Theory*, 106 (2016) 1-15.

[22] Q. L. Chen, C. S. Song, C. C. Zhu, X. S. Du and G. X. Ni, Manufacturing and contact characteristics analysis of internal straight beveloid gear pair, *Mechanism and Machine Theory*, 114 (2017) 60-73.

Huang Yucheng is a M.S. candidate at the State Key Laboratory of Mechanical Transmissions, Chongqing University, China. His research area is meshing stiffness and dynamic analysis of precision transmission.

Du Xuesong, born in 1970, is currently an Associate Professor in School of Mechanical Engineering, Chongqing University, China. His research interests include mechanical design and mechanical system dynamics analysis.